High Entropy Nonlinear Dielectrics with Superior Thermally Stable Performance

Yong-Jyun Wang, Hung-Chi Lai, Yu-Ang Chen, Rong Huang, Ti Hsin, Heng-Jui Liu, Ruixue Zhu, Peng Gao, Cong Li, Pu Yu, Yi-Chun Chen, Jiangyu Li, Yi-Cheng Chen, Jien-Wei Yeh, and Ying-Hao Chu*

A high configurational entropy, achieved through a proper design of compositions, can minimize the Gibbs free energy and stabilize the quasi-equilibrium phases in a solid-solution form. This leads to the development of high-entropy materials with unique structural characteristics and excellent performance, which otherwise could not be achieved through conventional pathways. This work develops a high-entropy nonlinear dielectric system, based on the expansion of lead magnesium niobate–lead titanate. A dense and uniform distribution of nano-polar regions is observed in the samples owing to the addition of Ba, Hf, and Zr ions, which lead to enhanced performance of nonlinear dielectrics. The fact that no structural phase transformation is detected up to 250 °C, and no noticeable change or a steep drop in structural and electrical characteristics is observed at high temperatures suggests a robust thermal stability of the dielectric systems developed. With these advantages, these materials hold vast potential for applications such as dielectric energy storage, dielectric tunability, and electrocaloric effect. Thus, this work offers a new high-entropy configuration with elemental modulation, with enhanced dielectric material features.

1. Introduction

In the push for next-generation technology, unconventional materials with complex compositions play a significant role in achieving desired functionalities.[1] For example, designing novel high-entropy oxides (HEO) for various applications has been an intriguing research direction since 2015.[2,3] With a synthetic multi-component solid solution with more than five types of cations, outstanding phase stability could be achieved via the enhancement of configurational entropy, especially for high-temperature structures.[4,5] To date, various novel HEOs have been successfully synthesized, including solid electrolytes,[6] colossal dielectric constants,[7] Li-ion[8] and Na-ion batteries,[9] and CO_2/CO catalysts[10] which not only leverage an ensemble of properties from their multiple constituents

Y.-J. Wang, Y.-C. Chen, J.-W. Yeh, Y.-H. Chu
Department of Materials Science and Engineering
National Tsing Hua University
Hsinchu 30013, Taiwan
E-mail: yhchu@mx.nthu.edu.tw

H.-C. Lai, Y.-H. Chu
Department of Materials Science and Engineering
National Yang Ming Chiao Tung University
Hsinchu 30010, Taiwan

Y.-A. Chen, R. Huang
Key Laboratory of Polar Materials and Devices (MOE) and Department of Electronics
East China Normal University
Shanghai 200062, China

T. Hsin
Department of Materials
Imperial College London
London SW7 2AZ, UK

H.-J. Liu
Department of Materials Science and Engineering
National Chung Hsing University
Taichung 40227, Taiwan

R. Zhu, P. Gao
International Center for Quantum Materials
School of Physics
Peking University
Beijing 100871, China

R. Zhu, P. Gao
Electron Microscopy Laboratory
School of Physics
Peking University
Beijing 100871, China

C. Li, P. Yu
State Key Laboratory of Low Dimensional Quantum Physics and Department of Physics
Tsinghua University
Beijing 100084, China

Y.-C. Chen
Department of Physics
National Cheng Kung University
Tainan 701401, Taiwan

J. Li
Department of Materials Science and Engineering
Southern University of Science and Technology
Shenzhen, Guangdong 518055, China

but also offer numerous promising features superior to those of known materials.

The configuration entropy of a mixture of components increases with the addition of more equimolar principal elements into the system; this phenomenon led to the concept of high entropy. The addition of multi-components to a material is expected to result in a rearrangement of the interior microstructure and is accompanied by an evident change in the material properties.[11–13] For example, an increase in thermal stability is more significant in high-entropy stabilized materials than in others. Yang et al.[14] have designed a high-entropy stabilized $Bi_2Ti_2O_7$-based dielectric film, and demonstrated that its energy density (U_e) could reach ≈90 J cm^{-3} in the range of −100–150 °C. Thus, this process maximizes energy storage performance in a relatively high-temperature range. Sarkar et al.[15] have reported on the reversible lithium storage properties of HEOs, and demonstrated how the stabilization effect of high entropy could bring significant benefits for storage capacity retention and cycling stability. Thus, these studies have established remarkable opportunities for gaining excellent energy storage performance through multi-component designs. Therefore, the effect of compositional disorder on order parameter coupling in high-entropy systems has become a critical area to be understood and invoked various fundamental and applied interests. Disorder in atomic arrangements has been realized as a vital concept to understand the underlying physics of phenomena emerging from complex interactions of order parameters.

To verify the aforementioned concepts, $Pb(Mg,Nb)O_3$-$PbTiO_3$ (PMN-PT) with multi-elements in ABO_3 is an excellent candidate for further investigation. Extensive research[16–19] related to PMN-PT has highlighted its wide-ranging physical properties, especially its excellent piezoelectric response. Various applications have been soon developed such as actuators,[20] ultrasonic transducers,[21] and energy harvesting devices.[22] However, the relatively low curie temperature (≈150 °C) of PMN-PT severely constrains the operational temperature range and life span under long-term usage. Introducing the high-entropy concept with enhanced thermal stability promises an exciting direction to pursue new materials with improved functionalities. In this work, ions of barium (Ba), hafnium (Hf), and zirconium (Zr) were added to an initial PMN-PT configuration with elemental modulation. We fabricated variously oriented single-crystal-like $(Pb_xBa_{1-x})(Mg_{0.15}Nb_{0.3}Ti_{0.05}Hf_{0.25}Zr_{0.25})O_3$ (PMNTBHZO) films on $SrTiO_3$ (STO) substrates, where x denotes the adjustable Ba amount, [Ba]. One reason for the selection of Ba, Hf, and Zr is that the choices for the B-site elements in perovskite dielectrics are limited, considering the valence state. Furthermore, Hf and Zr were selected because $PbHfO_3$[23] and $PbZrO_3$[24] are stable perovskites with nonlinear dielectric properties and low leakage. On the other hand, [Ba] helps enhance the A-site disorder arrangement and further increases the overall configurational entropy. With this consideration, in this work, Hf, Zr, and Ba were selected and they were expected to establish a stable high entropy. In a nutshell, the multi-component feature in the synthesized system results in an increase in the overall configurational entropy, leading to enhanced thermal stability. Specifically, the more stable crystal structure can be ascribed to the high-entropy-induced sluggish diffusion effect, which means that the diffusion of individual elements in composites with higher configurational

entropy of mixing should be slower than that in composites with lower configurational entropy. However, the electrical properties are usually strongly related to structural factors, especially for non-linear dielectric materials. Therefore, this new solid solution is expected to exhibit superior temperature stability of structural and dielectric characteristics.

The epitaxial relationships between the films and substrates were characterized by X-ray diffraction (XRD) and transmission electron microscopy (TEM). The severe lattice disorder led to the disappearance of phase transformation and denser distribution of nano-polar regions.[25,26] Considering this fact, various intriguing applications, based on these properties were further investigated, as shown in **Figure 1**a; these include dielectric energy storage, dielectric tunability, and electrocaloric (EC) effect. We identified a frequency-dependent dielectric constant for the relaxor ferroelectric characteristic at different temperatures. In contrast, the anisotropic behavior in the dielectric energy storage with excellent thermal stability was characterized by in situ electrical measurements with temperature dependence, thereby broadening the practical applications of HEOs.

2. Results and Discussion

2.1. Structural Characteristics of Epitaxial HEOs

First, the structural characteristics of high-entropy PMNTHZO and PMNTBHZO films on single crystal $SrTiO_3$ (STO) (100) substrates were identified by XRD. The reciprocal space maps (RSMs) of these two types of films around the (103) reflections of STO (001) substrates are shown in Figures 1b,c, respectively. Both RSMs exhibit spotty patterns for films and substrates, indicating a single-crystal-like crystallinity in the HEOs with a clear epitaxial relationship between the films and substrates. The in-plane and out-of-plane lattice constants for (001)-oriented PMNTHZO and PMNTBHZO films were calculated from the diffraction spots around STO (103) to be ≈4.110 Å. Moreover, the RSMs of (013) reflections are also provided in Figure S1, Supporting Information. The close reflections suggest the same in-plane lattice parameters. It implies that the PMNTHZO and PMNTBHZO films possessed a pseudocubic structure and presented a nearly strain-relaxed state. Similar results were observed through XRD θ–2θ scans for the PMNTHZO films grown on substrates with various orientations, namely (100), (110), and (111), as shown in Figure S2, Supporting Information; here all the films show approximately the same lattice constants. The phi-scans for these differently oriented PMNTHZO films were also recorded along (202), (200), and (200) reflections of STO (100), (110), and (111) substrates. These films showed the same symmetry with the substrates, confirming that all of them had excellent epitaxial relationships. The epitaxy nature can also be observed through cross-sectional TEM images (Figure S3, Supporting Information). Moreover, the thermal influence on the structure is worth investigating for this high-entropy system. The expansion of the c-axis from the in situ high-temperature XRD analysis, illustrated in Figure 1d reveals the structural thermostability values of PMNTHZO (yellow dots) and PMNTBHZO (blue dots); these were compared to that of the synthesized parent phase of PMN-PT (red dots). The abrupt increase in the c-axis for PMNTHZO in Figure 1d suggests that the phase transition of PMNTHZO

ADVANCED
SCIENCE NEWS

www.advancedsciencenews.com

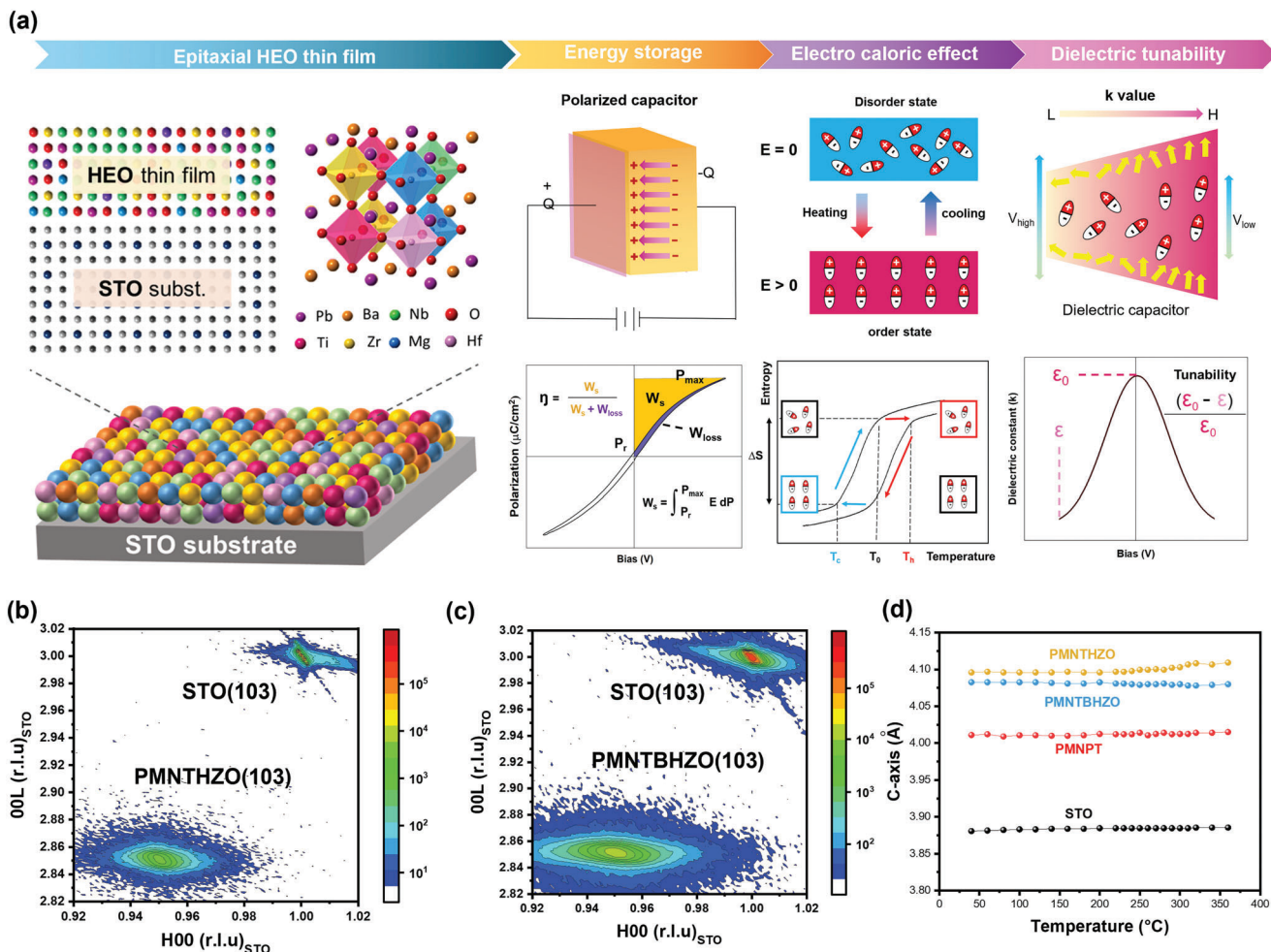**ADVANCED**
MATERIALS

www.advmat.de

Figure 1. a) The schematic diagram of the epitaxial high entropy oxide relaxor thin film and related energy storage, dielectric tunability, and dye degradation applications. b,c) The reciprocal spacing mapping of PMNTHZO and PMNTBHZO on STO substrate. d) Thermal expansion in the c-axis of PMNTHZO and STO substrate with temperature dependence.

occurred at 270 °C, while the phase transition for the synthesized PMN-PT can be observed at ≈200 °C. However, there is no noticeable change for the *c*-axis of PMNTBHZO, meaning that [Ba] significantly modulated the thermal stability up to higher than 350 °C. Furthermore, the phase of PMNTBHZO was stable even at a temperature of 600 °C, as shown in Figure S4, Supporting Information. This result suggests that the sluggish diffusion effect in this multi-component system weakened the phase transition, thereby causing a non-obvious change in the crystal structure. With this structure, the thermal stability of the related electrical properties is expected to be improved and render the structure suitable for practical applications.

Furthermore, to examine the chemical homogeneity, interfacial diffusion, and entropy-stabilized microstructures of the PMNTHZO and PMNTBHZO films on $SrRuO_3$ (SRO) coated STO substrates, high-angle annular dark-field scanning transmission electron microscopy (HAADF-STEM) investigations were conducted with atomic resolution and elemental sensitivity. **Figure 2**a shows the atomically resolved energy dispersive spectroscopy (EDS) maps of all the elements in the PMNTBHZO thin film. Pb and Ba atoms occupied the A-site, while Mg, Ti, Zr, Nb,

and Hf atoms randomly occupied the B-site with slight fluctuations, as has been already reported in the literature.[2] These results unambiguously reveal the feature of high-entropy materials composed of five elements at the same lattice site (here the B-site atoms, i.e., Mg, Ti, Zr, Nb, and Hf). Considering the entropy-stabilized structure and variant ionic radii for different ions, the existence of nano-domain regions with relaxor-like polarization is expected for the PMNTHZO and PMNTBHZO films. Figure 2b,c shows a typical HAADF-STEM image and the corresponding polarization vector map of PMNTBHZO film along the [100] direction. Nano-domain regions with sizes of 1–5 nm can be clearly distinguished, which are indicated by the dashed ellipses with arrows of polarization direction. An enlarged nano-domain region is shown in Figure 2d, which shows the local polarization direction. The diverse atomic displacements between the A and B sites (in ABO_3 perovskite structure), distributed at different nano-regions represent the typical characteristic of relaxor ferroelectrics; this is explained by the polar slush model, which says that chemical inhomogeneity with a significant lattice distortion prohibits the polarization rotation and results in low-angle domain walls.[27]
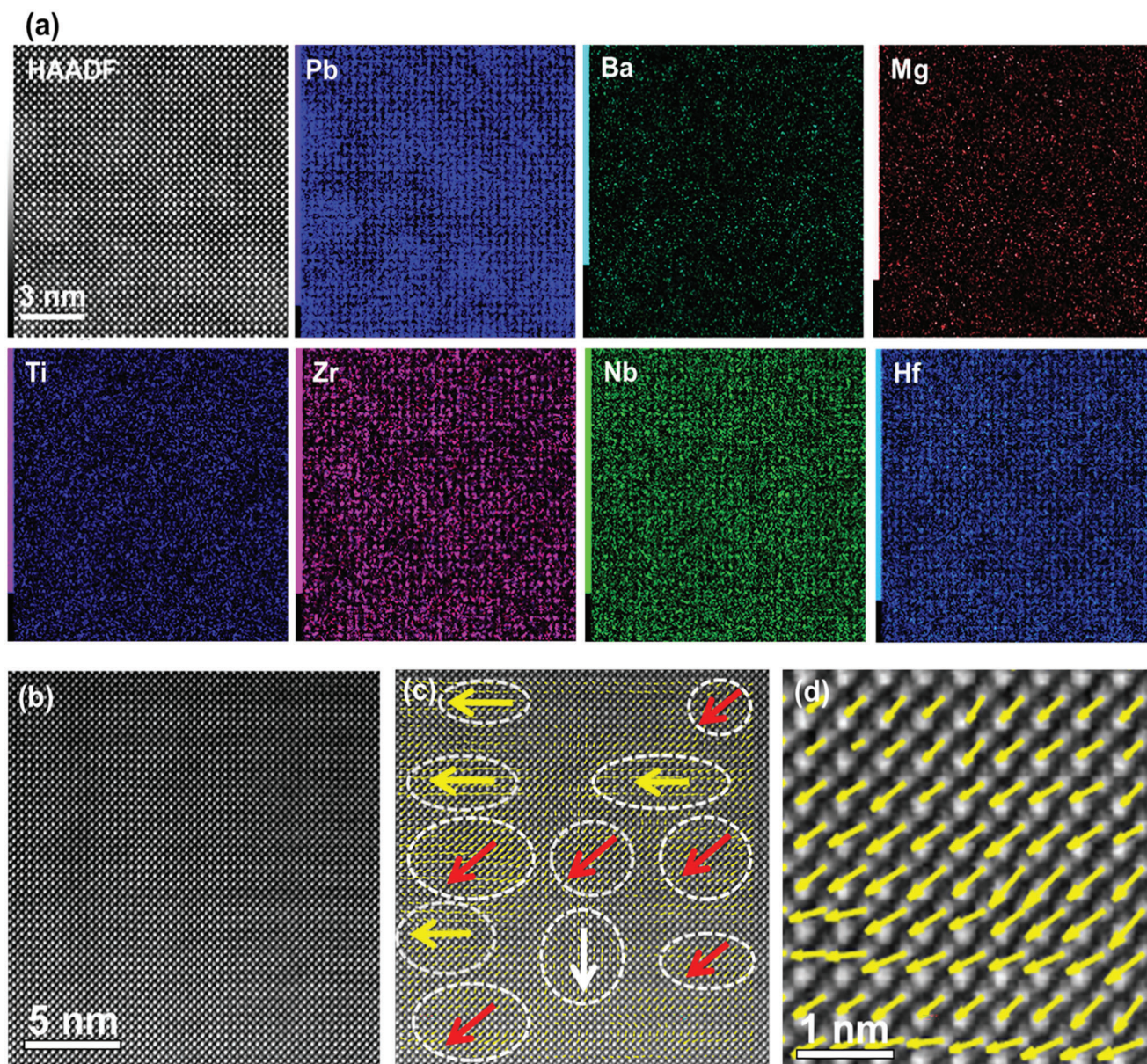
**ADVANCED
SCIENCE NEWS**

www.advancedsciencenews.com

**ADVANCED
MATERIALS**

www.advmat.de

Figure 2. a) Atomically resolved HAADF image and corresponding elemental mapping of the HEO thin film. b) A typical HAADF-STEM image and c) corresponding polarization vector map of PMNTBHZO film along the [100] direction. d) An enlarged nano-domain region exhibiting the local polarization direction.

2.2. Thermal Stability of Electrostatic Energy Storage of PMNTHZO with Anisotropic Orientation and Influence of Ba Ions

Extensive studies revealed the enormous potential of ferroic HEOs in electrostatic energy storage applications; this is because a dense distribution of nano-domain boundaries not only serves as a nano depletion region,[28] but also increases the potential barriers for charge transport, resulting in higher resistivity and permittivity.[29,30] Additionally, most ferroic HEOs benefit from the complexity of composition with a significant lattice distortion, possessing relaxor ferroelectric characteristics with large saturated polarization (high U_e) and slim hysteresis loop (high effi-

ciency, η);[31,32] these characteristics are favorable for their application in dielectric energy storage. The long-standing bottleneck for dielectric energy storage capacitors is their relatively small U_e. To solve this problem, previous researchers have reported methods for increasing U_e, which can be classified into two categories: 1) the use of additional components and 2) the incorporation of nano-domain modifications. Acharya et al.[33] synthesized a $Pb_xSr_{1-x}HfO_3$ thin film to gain a higher U_e ($\approx$77 J cm^{-3}); Wang et al.[34] showed that $(Ba_{0.95},Sr_{0.05})(Zr_{0.2},Ti_{0.8})O_3$ ultracapacitors exhibited a high recyclable U_e ($\approx$100 J cm^{-3}). These reports extensively demonstrated how the additional components affected the U_e performance. On the other hand, modifying the nanodomain is another effective way to increase U_e. For example, Chen et al.[35]
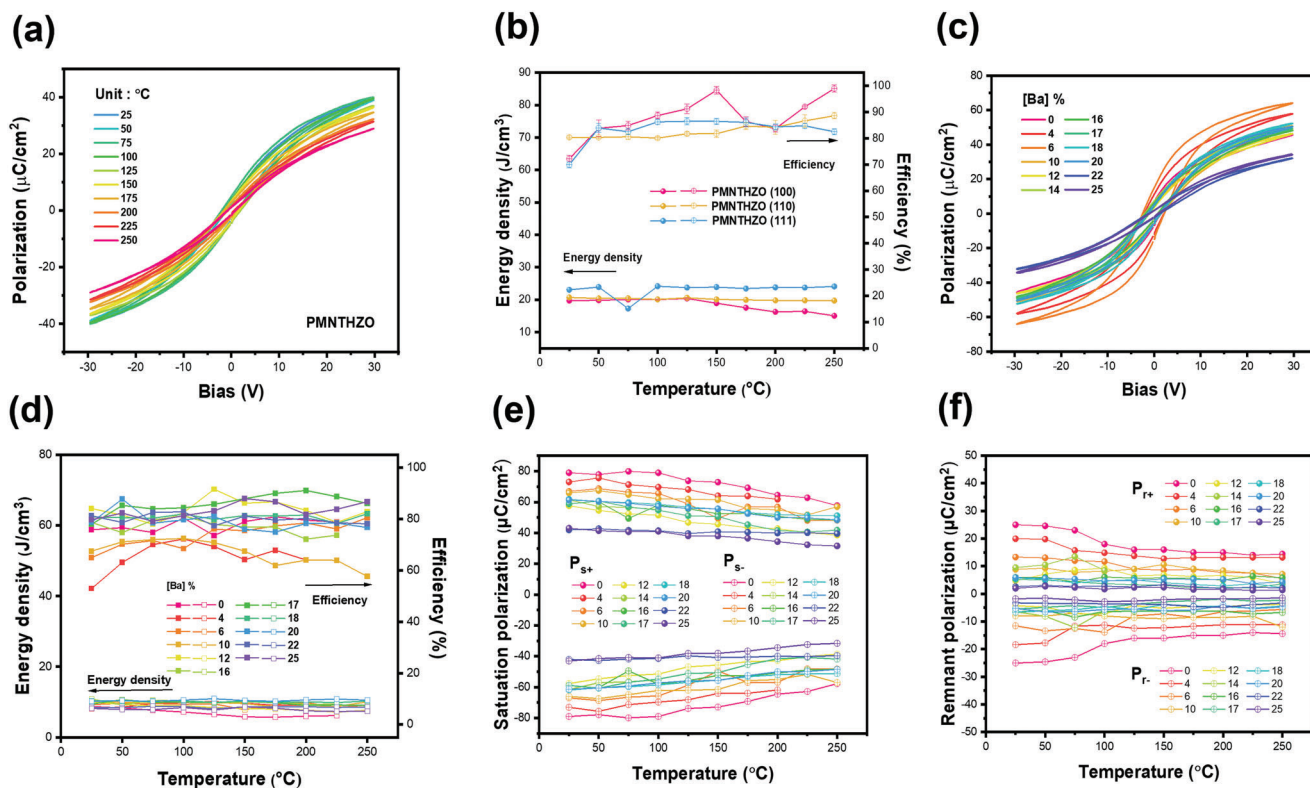
ADVANCED
SCIENCE NEWS
www.advancedsciencenews.com

ADVANCED
MATERIALS
www.advmat.de

Figure 3. a) Temperature-dependence polarization (*P*)–voltage (*V*) hysteresis loops collected from PMNTHZO thin film on STO. b) Calculated energy density and efficiency with temperature dependence. c) Ba-doped level dependence *P*–*V* hysteresis loops collected from PMNTHZO thin film on STO. d) Calculated energy density and efficiency of c) with temperature dependence. e,f) Saturation and remnant polarization of the Ba-doped level dependence *P*–*V* hysteresis loops.

showed that a high U_e (>10 J cm^{-3}) could be obtained by using high-entropy KNN-based ceramics. Pan et al.[25,32,36] reported obtaining ultra-high U_e values by controlling the nano-domain design in BiFeO$_3$-based materials. However, less attention was paid to studying the thermal stability of performance, which is a critical parameter for practical applications and can be a significant advantage of the high-entropy effect. Owing to the high power and long-term usage, the internal thermal energy was not negligible during the operation.

The indicators η and U_e are essential to evaluate the performance of high-entropy materials for high energy storage dielectric capacitors. These are calculated from Equations (1) and (2) below

$$\text{Energy density} = -\int_{P_{max}}^{P_r} E dP \tag{1}$$

$$\text{Energy storage efficiency} = \frac{\text{dischargeable energy density}}{\text{dischargeable energy} + \text{energy loss}} \tag{2}$$

Taking advantage of the nano-sized domains with low-angle domain walls in PMNTHZO HEO, the energy loss in domain switching was relatively low, resulting in a much smaller coercive field than in classical ferroelectrics. The polar nano-regions were sensitive to external bias; yet, they displayed relatively low remnant polarization, and therefore, PMNTHZO presented a good

performance in electrostatic energy storage. Although these polar nano-domains have been proposed to be the primary mechanism for an improved relaxor behavior, these were initially thought to be below T_d. Some more studies have also revealed that the crystal orientation would influence the related properties. Notably, we observed the excellent thermal stability of the PMNTHZO heterostructure. **Figure 3**a shows the temperature-dependent polarization (*P*)–voltage (*V*) hysteresis loops of the PMNTHZO films with a thickness of ≈400 nm. U_e and η of the (100)-, (110)-, and (111)-oriented PMNTHZO films were calculated and plotted in Figure 3b. According to this figure, the (110)-oriented PMNTHZO film exhibited the most stable thermal stability in the temperature range of 25–250 °C. Such an inconspicuous attenuation revealed the better thermal stability of the (110)-oriented PMNTHZO film than that of either the (100)- or (111)-oriented HEO films. On the other hand, to investigate the impact of the Ba element, the *P*–*V* loops with [Ba] of up to 25% are plotted in Figure 3c. At room temperature, the actual polarization behavior of the PMNTHZO gradually changed from a ferroelectric state to a relaxor one, with increasing [Ba]. This fact was verified via the Curie–Weiss fitting in Figure S5, Supporting Information. As a result, U_e, η, saturation, and remnant polarization could be modified, as shown in Figure 3d–f. Compared to the regular PMN-PT film (Figure S6, Supporting Information), U_e and η were improved. The variation in the energy storage performance was reduced owing to the thermal stability, and the endurance
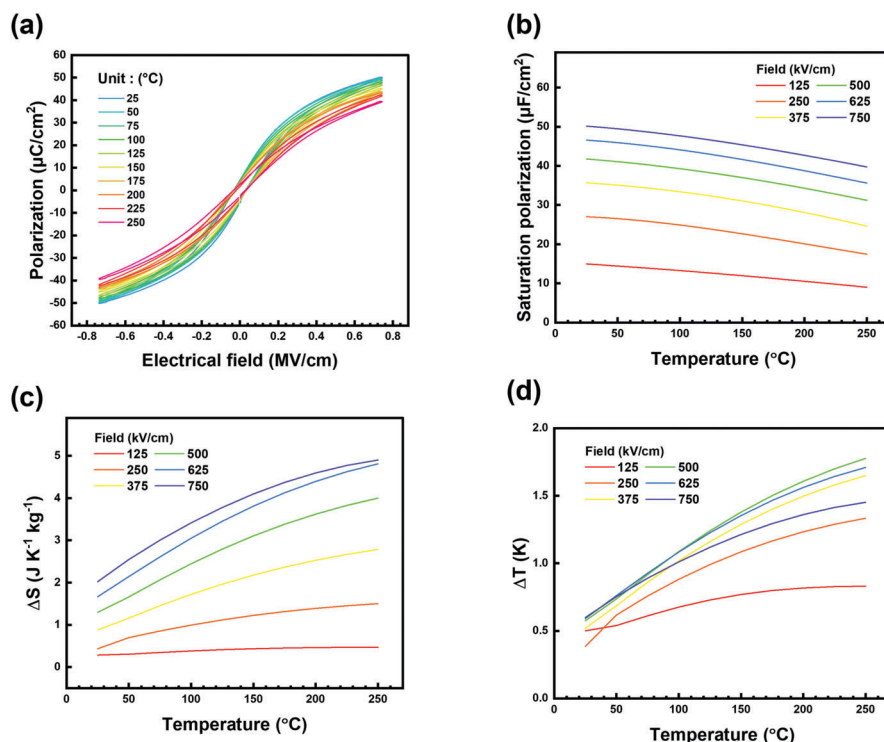
Figure 4. Electrocaloric effect of PHMTHZO thin film. a) The temperature dependence P–V loops under 750 kV cm^{-1}. b) The temperature-dependence saturation polarization under different electric fields. The electric-field-driven c) entropy and d) temperature change under different electric fields.

temperature increased to 250 °C when [Ba] reached 18%, thus showing excellent thermal stability. Moreover, a comparison with other reported works is shown in Table S1[40], Supporting Information, which reveals no significant improvement for the synthesized PMNTHZO and PMNTBHZO thin films compared to other dielectric systems. These efforts suggest the significant potential for gaining excellent energy storage performance through the additional components and introduction of a high-entropy design. However, less attention was paid to studying the thermal stability of performance, which is a critical parameter for practical applications. This motivated us to focus more on this problem. A <1% variation could be obtained for U_e and η in the temperature range of 25–250 °C, suggesting robust thermal stability for energy storage. Indeed, the thermal stability of the synthesized HEO thin film was outstanding compared to that of others. For the synthesized PMNTHZO and PMNTBHZO systems, the electrical properties showed a significant improvement compared to the original PMN-PT, confirming the phase transition. Owing to their high-entropy stabilized structure, the synthesized PMNTB-HZO and PMNTHZO films exhibited enhanced thermal stability, which is beneficial for high-temperature and long-term operations. In summary, this led to the conclusion that adding Ba, Hf, and Zr in the HEO system significantly minimized the influence of temperature.

2.3. Electrocaloric Effect of PMNTBHZO Thin Film

In addition to energy storage, the demand for a highly efficient and environmentally friendly solid-state cooling technol-

ogy has been rising recently. Therefore, the concept of caloric effect has been rapidly developed, which refers to a change in the temperature under an adiabatic application of external fields.[37] This technique alters the traditional vapor-compression cooling method, which offers an environmentally friendly pathway without the involvement of harmful coolants. Based on the structural and electrical measurements, it was confirmed that Ba ions could stabilize the transition behavior. The PMNTBHZO thin film exhibited a non-obvious phase transformation compared to the traditional ferroelectric materials. Thus, the electrocaloric effect was further explored to study the excellent thermal stability of the PMNTBHZO film. The electric field was varied from 125 to 750 kV cm^{-1} to investigate the performance under different driving strengths. The temperature-dependent P–E curves under an electric field of 750 kV cm^{-1} are shown in **Figure 4**a, and the temperature-dependent saturation polarization under different electric fields is presented in Figure 4b. Compared to the ferroelectric to paraelectric phase transformation of traditional ferroelectric materials, the PMNTBHZO film retained the polarization behavior of a typical relaxor body. Furthermore, the saturation polarization increased with an increasing electric field. Next, to quantify the performance of the EC effect, the caloric effect (electric field-induced ΔS, ΔT) was obtained by numerically computing the following integrals

$$\Delta S = -\frac{1}{\rho} \int_{E1}^{E2} \left(\frac{\partial Ps}{\partial T} \right) dE \tag{3}$$

$$\Delta T = -\frac{1}{\rho} \int_{E1}^{E2} \frac{T}{C} \left(\frac{\partial Ps}{\partial T} \right) dE \tag{4}$$

**ADVANCED
SCIENCE NEWS**

www.advancedsciencenews.com
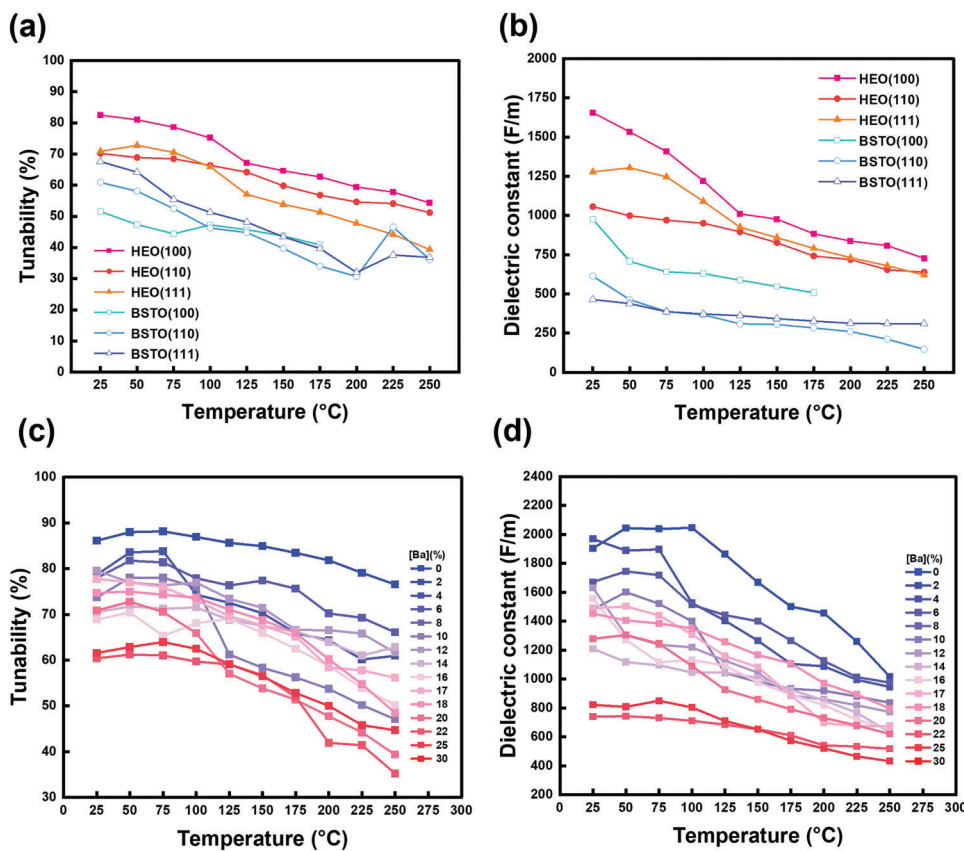
**ADVANCED
MATERIALS**

www.advmat.de

Figure 5. a,b) Comparison of the tunability and dielectric constant between HEO and BSTO thin film with orientation anisotropy, and c,d) with Ba-doped level dependence.

It may be noted that the above equations need to be revised for thin films. Thus, the values obtained from the calculations are relative rather than absolute. Based on the analysis, the temperature-dependent electric-field induced ΔS and ΔT are shown in Figures 4c,d, respectively. The maximum ΔS was ≈ 4.7 J K^{-1} Kg^{-1} under 750 kV cm^{-1}, and the maximum ΔT was 1.75 K under 500 kV cm^{-1}. The smooth variation in ΔS and ΔT with increasing temperature can be observed from the results, which demonstrate that the HEO system could successfully offer a comprehensive range of EC effects and potential for a broad range of applications.

2.4. Temperature-Dependency of Dielectric Properties of PMNTBHZO Thin Film and Influence of Ba Ions

After realizing the polarization behavior of the high-entropy films, attention was next paid to dielectric tunability, which is significant in many practical applications such as tunable antennas[38] and microwave circuits.[39] The most common material with a high dielectric tunability is $Ba_xSr_{1-x}TiO_3$ (BSTO), whose dielectric tunability is $\approx 50\%$; this is significantly higher than that of most nonlinear dielectric materials. However, its severe performance drop in high-temperature operations hinders its use in high-power and long-duration applications. **Figure 5**a shows the temperature-dependent dielectric tunability of the PM-

NTBHZO and $Ba_{0.5}Sr_{0.5}TiO_3$ (BSTO) films with the same thicknesses, but different orientations. The capacitance–electric field (C–E) curves in Figure S7, Supporting Information, show that a single peak appears at the zero electric field position. The (111)-oriented PMNTBHZO film shows the most extensive tunability, which could be regulated from 80% to 68% when the temperature increased from room temperature to 200 °C. For the BSTO film, the (110) orientation exhibits the most stable thermal stability with an average tunability of $\approx 50\%$, for a temperature of up to 175 °C. The high-entropy PMNTBHZO film exhibited larger tunability and superior thermal stability than the BSTO film, offering a pathway to obtain enhanced physical properties for multi-elemental designs. A similar situation can be observed in the dielectric constant in Figure 5b. The dielectric constant of (100)-oriented PMNTBHZO ranged from 1121 to 741 (33.8% decay) when the temperature was up to 250 °C. However, the dielectric constant of (100)-oriented BSTO film varied from 973 to 562 (42.2% decay) when the temperature increased to 175 °C. The high-entropy feature increased the thermal stability and improved the dielectric properties. Additionally, the influence of [Ba] was also investigated and is shown in Figure 5c,d. A significant decay in the tunability and dielectric constant could be seen with an increase in [Ba], suggesting a practical pathway to finely calibrate the dielectric properties through an elemental control. Furthermore, a comparison of the dielectric tunability between different dielectric systems is shown in Table S2[41–44], Supporting

**ADVANCED
SCIENCE NEWS**

www.advancedsciencenews.com

**ADVANCED
MATERIALS**

www.advmat.de

Information, according to which, larger values of dielectric tunability can be seen in the synthesized PMNTHZO and PMNTBHZO films. Moreover, the thermal stability and temperature endurance were also enhanced by the introduction of a high-entropy design.

3. Conclusion

In this study, we presented a new group of HEOs, namely the PMNTHZO relaxor ferroelectric films, with high electrostatic energy storage capacity, electrocaloric effect, and dielectric tunability. The fabricated PMNTHZO and PMNTBHZO films presented single-crystal-like crystallinity with uniform elemental distribution and polar nano-regions with varying polarization directions. In terms of electrostatic energy storage, the films exhibited outstanding energy density (6 J cm^{-3}) and thermal stability of storage efficiency (remained 65% at 175 °C), thus making them a promising choice for high-temperature energy storage. This performance can be ascribed to numerous polar nano-domains inside the films containing low-angle domain walls with high mobility that are sensitive to an external bias and yet have considerably small remnant polarization. Moreover, we investigated the influence of Ba ions on electrostatic energy storage. It is evident that the additional Ba ions significantly stabilized energy density and efficiency with temperature. Furthermore, the performance was improved when the Ba addition was 18% owing to the improved electrostatic energy storage behavior (energy density of 10 J cm^{-3} and storage efficiency of 82% at 250 °C). The electrocaloric effect of the HEO thin film was studied next to compare the same with that of conventional ferroelectric or antiferroelectric materials. In contrast to the noticeable ordinary phase transformation, the HEO thin film showed no critical transition temperature in the results of structural and electrical measurements. The electric field-driven ΔS and ΔT showed a stable behavior even when the temperature exceeded 175 °C, suggesting very high thermal stability for more practical uses. Finally, the dielectric tunability of the HEO film was also investigated, along with the influence of Ba ions. Compared to the BSTO thin films, the PMNTBHZO thin film showed a larger dielectric tunability of more than 10%. Moreover, the thermal stability was also conspicuously improved with a temperature tolerance of greater than 250 °C, which can be attributed to the intrinsic merit of high entropy. Finally, this study utilized the advantage of structural and electrical stability of HEOs for electrostatic energy storage, electrocaloric effect, and dielectric tenability, and shed light on exploring the novel HEOs for improved dielectric functionalities.

4. Experimental Section

Sample Preparation: The PMNTHZO/SRO/STO thin films were fabricated via pulsed laser deposition with commercial PMNTHZO and SRO targets (SRO was the bottom electrode for electrical analysis). Commercial STO single crystals were used as the substrates. The vacuum chamber was evacuated to a pressure of 1×10^{-6} Torr before deposition. First, SRO was grown on the substrate at 680 °C under 100 mTorr of O_2 pressure. Second, PMNTHZO was deposited under the same pressure when the substrate was cooled down to 580 °C. Finally, the annealing process was operated at 580 °C with 100 Torr of O_2 pressure, followed by a cooling rate of 0.3 °C s^{-1}. To fabricate PMNTBHZO thin film, the dual-target deposi-

tion on STO (100) with PMNTHZO and BHZO targets was adopted. The pulsed number of the laser can control the amount of additional Ba. First, SRO was grown on the substrate at 680 °C under 100 mTorr of O_2 pressure. Second, dual-target deposition for PMNTHZO and BHZO was conducted under the same pressure when the substrate was cooled down to 580 °C. Finally, the annealing process was operated at 580 °C with 100 Torr of O_2 pressure, followed by a cooling rate of 0.3 °C s^{-1}.

X-ray Diffraction: High-resolution XRD techniques were performed to verify the crystal structures and epitaxial relationships of the HEO films. Typical θ–2θ scans along surface normal directions of substrates were carried out by Bruker D2 Discover System with Cu Kα X-ray ($\lambda = 1.5406$ Å). RSMs and phi-scans were recorded using Bruker D8 advance XRD system with the same X-ray source. The RSMs were plotted in the reciprocal lattice units normalized to the d-spacings of STO substrates.

Transmission Electron Microscopy Characterization and Analysis: HAADF-STEM images and EDS mapping were acquired on a JEOL ARM300, capable of recording high-resolution STEM images with a spatial resolution of 63 pm. The microscope was equipped with a double spherical aberration (CS) corrector and an X-ray energy dispersive spectrometer (JED-2300 Series) with two 158 mm^2 Silicon Drift Detectors (SDD). HAADF image was acquired with a probe convergence angle of 24 mrad and a collection angle of ≈64 mrad. In the present STEM-EDS characterization, a fine electron probe was used. The CL aperture was 30 um with a probe current of about 35 pA. The samples were robust under the present experimental conditions. The total collection time was 15 min. To calculate the unit-cell-wise polarization, the position of each cation was determined by simultaneous fitting with 2D Gaussian peaks using MATLAB code.[45] Then the map of the displacement vector between A and B sites (for ABO$_3$ perovskite structure) can be extracted accordingly.

Electrical Properties: The P–V measurements were performed under 100 mV AC voltage, 1 kHz AC frequency, and the voltage was measured from 40 to −40 V. The in situ temperature-dependent electrical properties were measured by a commercial instrument for ferroelectric properties (TFAnalyzer3000, aixACCT Systems).

Supporting Information

Supporting Information is available from the Wiley Online Library or from the author.

Conflict of Interest

The authors declare no conflict of interest.

Author Contributions

Y.-J.W., H.-J.L., and Y.-H.C. designed the experiments. H.-C.L. and T.H. synthesized the films and conducted structural characterization and electrical analysis of XRD and P–E measurements with temperature dependence. H.-J.L. performed the RSM analysis. R.Z. and Y.-A.C. performed the TEM, STEM, and EDS analysis. C.L. performed in situ XRD analysis. Y.-J.W., H.-J.L., P.G., P.Y., Y.-C.C., J.L., J.-W.Y., and Y.-H.C. contributed to the analysis and understanding of the data. Y.-J.W. wrote the core of the manuscript. R.H., P.G., P.Y., Y.-C.C., J.L., J.-W.Y., and Y.-H.C. supervised the research. All the authors contributed to the discussion and manuscript preparation and read the final manuscript.

Data Availability Statement

The data that support the findings of this study are available from the corresponding author upon reasonable request.

Keywords

dielectric materials, epitaxial thin film, high entropy, relaxor

[1] M. H. Tsai, J. W. Yeh, *Mater. Res. Lett.* **2014**, *2*, 107.
[2] J.-W. Yeh, *Ann. Chim. Sci. Mat.* **2006**, *31*, 633.
[3] C. Oses, C. Toher, S. Curtarolo, *Nat. Rev. Mater.* **2020**, *5*, 295.
[4] N. Dragoe, D. Bérardan, *Stem Cells Int.* **2019**, *366*, 573.
[5] J. W. Yeh, S. K. Chen, S. J. Lin, J. Y. Gan, T. S. Chin, T. T. Shun, C. H. Tsau, S. Y. Chang, *Adv. Eng. Mater.* **2004**, *6*, 299.
[6] D. Bérardan, S. Franger, A. Meena, N. Dragoe, *J. Mater. Chem.* **2016**, *4*, 9536.
[7] D. Bérardan, S. Franger, D. Dragoe, A. K. Meena, N. Dragoe, *Phys. Status Solidi RRL* **2016**, *10*, 328.
[8] A. Sarkar, L. Velasco, D. Wang, Q. Wang, T. G. alasila, L. de Biasi, C. Kübel, T. Brezesinski, S. S. Bhattacharya, H. Hahn, *Nat. Commun.* **2018**, *9*, 3400.
[9] H. Chen, W. Lin, Z. Zhang, K. Jie, D. R. Mullins, X. Sang, S. Z. Yang, C. J. Jafta, C. A. Bridges, X. Hu, *ACS Mater. Lett.* **2019**, *1*, 83.
[10] C. Zhao, F. Ding, Y. Lu, L. Chen, Y. S. Hu, *Angew. Chem., Int. Ed. Engl.* **2020**, *59*, 264.
[11] G. M. Tomboc, X. Zhang, S. Choi, D. Kim, L. Y. S. Lee, K. Lee, *Adv. Funct. Mater.* **2022**, *32*, 2205142.
[12] Y. Han, X. Liu, Q. Zhang, M. Huang, Y. Li, W. Pan, P. A. Zong, L. Li, Z. Yang, Y. Feng, *Nat. Commun.* **2022**, *13*, 2871.
[13] B. Zhao, Y. Du, Z. Yan, L. Rao, G. Chen, M. Yuan, L. Yang, J. Zhang, R. Che, *Adv. Funct. Mater.* **2023**, *33*, 2209924.
[14] B. Yang, Y. Zhang, H. Pan, W. Si, Q. Zhang, Z. Shen, Y. Yu, S. Lan, F. Meng, Y. Liu, H. Huang, J. He, L. Gu, S. Zhang, L. Q. Chen, J. Zhu, C. W. Nan, Y. H. Lin, *Nat. Mater.* **2022**, *21*, 1074.
[15] A. Sarkar, L. Velasco, D. Wang, Q. Wang, G. Talasila, L. de Biasi, C. Kübel, T. Brezesinski, S. S. Bhattacharya, H. Hahn, B. Breitung, *Nat. Commun.* **2018**, *9*, 3400.
[16] P. Lv, J. Qian, C. Yang, T. Liu, Y. Wang, D. Wang, S. Huang, X. Cheng, Z. Cheng, *Nano Energy* **2022**, *97*, 107182.
[17] Q. Li, Y. Liu, J. Liu, K. Song, H. Guo, F. Li, Z. Xu, *Adv. Funct. Mater.* **2022**, *32*, 2201719.
[18] Z. Fang, X. Jiang, X. Tian, F. Zheng, M. Cheng, E. Zhao, W. Ye, Y. Qin, Y. Zhang, *Adv. Opt. Mater.* **2021**, *9*, 2002139.
[19] F. Tian, Y. Liu, R. Ma, F. Li, Z. Xu, Y. Yang, *Appl. Acoust.* **2021**, *175*, 107827.
[20] X. Gao, J. Liu, B. Xin, H. Jin, L. Luo, J. Guo, S. Dong, Z. Xu, F. Li, *Sens. Actuators, A* **2021**, *331*, 113052.
[21] Y. Yang, K. Zhu, E. Sun, P. Liu, R. Zhang, W. Cao, *Sens. Actuators, A* **2022**, *346*, 113873.
[22] M. Ma, S. Xia, X. Gao, K. Song, H. Guo, F. Li, Z. Xu, Z. Li, *Appl. Phys. Lett.* **2022**, *120*, 042902.
[23] M. F. Tsai, Y. Z. Zheng, S. C. Lu, J. D. Zheng, H. Pan, C. G. Duan, P. Yu, R. Huang, Y. H. Chu, *Adv. Funct. Mater.* **2021**, *31*, 2105060.
[24] D. L. Ko, T. Hsin, Y. H. Lai, S. Z. Ho, Y. Zheng, R. Huang, H. Pan, Y. C. Chen, Y. H. Chu, *Nano Energy* **2021**, *87*, 106149.
[25] H. Pan, F. Li, Y. Liu, Q. Zhang, M. Wang, S. Lan, Y. Zhang, J. Ma, L. Gu, Y. Shen, P. Yu, S. Zhang, L. Q. Chen, Y. H. Lin, C. W. Nan, *Stem Cells Int.* **2019**, *365*, 578.
[26] H. Takenaka, I. Grinberg, S. Liu, A. M. Rappe, *Nature* **2017**, *546*, 391.
[27] R. Waser, R. Hagenbeck, *Acta Mater.* **2000**, *48*, 797.
[28] D. Li, D. Zhou, W. Liu, P. J. Wang, Y. Guo, X. G. Yao, H. X. Lin, *J. Chem. Eng.* **2021**, *419*, 129601.
[29] R. Xu, J. Karthik, A. R. Damodaran, L. W. Martin, *Nat. Commun.* **2014**, *5*, 3120.
[30] L. Wu, X. Wang, L. Li, *RSC Adv.* **2016**, *6*, 14273.
[31] B. Neese, B. Chu, S. G. Lu, Y. Wang, E. Furman, Q. Zhang, *Stem Cells Int.* **2008**, *321*, 821.
[32] H. Pan, F. Li, Y. Liu, Q. Zhang, M. Wang, S. Lan, Y. Zheng, J. Ma, L. Gu, Y. Shen, P. Yu, S. Zhang, L. Q. Chen, Y. H. Lin, C. W. Nan, *Stem Cells Int.* **2021**, *374*, 100.
[33] M. Acharya, E. Banyas, M. Ramesh, Y. Jiang, A. Fernandez, A. Dusgupta, H. Ling, B. Hanrahan, K. Persson, J. B. Neaton, L. W. Martin, *Adv. Mater.* **2022**, *34*, 2105967.
[34] K. Wang, J. Ouyang, M. Wuttig, Y. Y. Zhao, H. Cheng, Y. Zhang, R. Su, J. Yan, X. Zhong, F. Zeng, *Adv. Energy Mater.* **2020**, *10*, 2001778.
[35] L. Chen, S. Deng, H. Liu, J. Wu, H. Qi, J. Chen, *Nat. Commun.* **2022**, *13*, 3089.
[36] H. Pan, J. Ma, J. Ma, Q. Zhang, X. Liu, B. Guan, L. Gu, X. Zhang, Y. J. Zhang, L. Li, Y. Shen, Y. H. Lin, C. W. Nan, *Nat. Commun.* **2018**, *9*, 1813.
[37] V. Varadan, K. Jose, V. Varadan, *SMS* **1999**, *8*, 238.
[38] A. Ahmed, I. A. Goldthorpe, A. K. Khandani, *APR* **2015**, *2*, 011302.
[39] W. Gao, L. You, Y. Wang, G. Yuan, Y. H. Chu, Z. Liu, J. M. Liu, *Adv. Electron. Mater.* **2017**, *3*, 1600542.
[40] J. Kim, S. Saremi, M. Acharya, G. Velarde, E. Parsonnet, P. Donahue, A. Qualls, D. Garcia, L. W. Martin, *Stem Cells Int.* **2020**, *369*, 81.
[41] X. G. Tang, K. H. Chew, H. L. W. Chan, *Acta Mater.* **2004**, *52*, 5177.
[42] Z. Yuan, Y. Lin, J. Weaver, X. Chen, C. L. Chen, G. Subramanyam, J. C. Jiang, E. I. Meletis, *Appl. Phys. Lett.* **2005**, *87*, 152901.
[43] P. Ren, Z. Liu, Q. Wang, B. Peng, S. Ke, H. Fan, G. Zhao, *Sci. Rep.* **2017**, *7*, 6693.
[44] O. Lee, S. A. Harrington, A. Kursumovic, E. Defay, H. Wang, Z. Bi, C. F. Tsai, L. Yan, Q. Jia, J. L. MacManus-Driscoll, *Nano Lett.* **2012**, *12*, 4311.
[45] Q. Zhang, L. Y. Zhang, C. H. Jin, Y. M. Wang, F. Lin, *Ultramicroscopy* **2019**, *202*, 114.